Virtual $O(\alpha_s)$ corrections to the inclusive decay $b\to s\gamma$

Christoph Greub
Stanford Linear Accelerator Center, Stanford University, Stanford, California 94309

Tobias Hurth* and Daniel Wyler
Institute for Theoretical Physics, University of Zürich, Winterthurerstr. 190, CH-8057 Zürich, Switzerland
(Received 26 March 1996)

We present in detail the calculation of the $O(\alpha_s)$ virtual corrections to the matrix element for $b\to s\gamma$. In addition to the one-loop virtual corrections of the electromagnetic and color dipole operators O_7 and O_8, we include the important two-loop contribution of the four-Fermi operator O_2. By applying the Mellin-Barnes representation to certain internal propagators, the result of the two-loop diagrams is obtained analytically as an expansion in m_c/m_b. These results are then combined with existing $O(\alpha_s)$ bremsstrahlung corrections in order to obtain the inclusive rate for $B\to X_s\gamma$. The new contributions drastically reduce the large renormalization scale dependence of the leading logarithmic result. Thus, a very precise standard model prediction for this inclusive process will become possible once the corrections to the Wilson coefficients are also available. [S0556-2821(96)02017-6]

PACS number(s): 13.20.He, 11.10.Hi, 12.38.Bx

I. INTRODUCTION

In the standard model (SM), flavor-changing neutral currents only arise at the one-loop level. This is why the corresponding rare B meson decays are particularly sensitive to ''new physics.'' However, even within the standard model framework, one can use them to constrain the Cabibbo-Kobayashi-Maskawa (CKM) matrix elements which involve the top quark. For both these reasons, precise experimental and theoretical work on these decays is required.

In 1993, $B\to K^*\gamma$ was the first rare B decay mode measured by the CLEO Collaboration [1]. Recently, also the first measurement of the inclusive photon energy spectrum and the branching ratio in the decay $B\to X_s+\gamma$ was reported [2]. In contrast with the exclusive channels, the inclusive mode allows a less model-dependent comparison with theory, because no specific bound state model is needed for the final state. This opens the road to a rigorous comparison with theory.

The data agrees with the SM-based theoretical computations presented in [3–5], given that there are large uncertainties in both the experimental and the theoretical results. In particular, the measured branching ratio $B(B\to X_s\gamma)=(2.32\pm 0.67)\times 10^{-4}$ [2] overlaps with the SM-based estimates in [3,4] and in [6,7].

In view of the expected increase in the experimental precision, the calculations must be refined correspondingly in order to allow quantitative statements about new physics or standard model parameters. So far, only the leading logarithmic corrections have been worked out systematically. In this paper we evaluate an important class of next order corrections, which we will describe in detail below.[1]

We start within the usual framework of an effective theory with five quarks, obtained by integrating out the heavier degrees of freedom which in the standard model are the top quark and the W boson. The effective Hamiltonian includes a complete set of dimension-6 operators relevant for the process $b\to s\gamma$ (and $b\to s\gamma g$) [9]:

$$H_{\rm eff}(b\to s\gamma)=-\frac{4G_F}{\sqrt{2}}\lambda_t\sum_{j=1}^{8}C_j(\mu)O_j(\mu), \qquad (1.1)$$

with G_F being the Fermi coupling constant and $C_j(\mu)$ being the Wilson coefficients evaluated at the scale μ, and $\lambda_t=V_{tb}V_{ts}^*$ with V_{ij} being the CKM matrix elements. The operators O_j are

$$\begin{aligned}
O_1&=(\overline{c_{L\beta}}\gamma^\mu b_{L\alpha})(\overline{s_{L\alpha}}\gamma_\mu c_{L\beta}),\\
O_2&=(\overline{c_{L\alpha}}\gamma^\mu b_{L\alpha})(\overline{s_{L\beta}}\gamma_\mu c_{L\beta}),\\
O_3&=(\overline{s_{L\alpha}}\gamma^\mu b_{L\alpha})[(\overline{u_{L\beta}}\gamma_\mu u_{L\beta})+\cdots+(\overline{b_{L\beta}}\gamma_\mu b_{L\beta})],\\
O_4&=(\overline{s_{L\alpha}}\gamma^\mu b_{L\beta})[(\overline{u_{L\beta}}\gamma_\mu u_{L\alpha})+\cdots+(\overline{b_{L\beta}}\gamma_\mu b_{L\alpha})],\\
O_5&=(\overline{s_{L\alpha}}\gamma^\mu b_{L\alpha})[(\overline{u_{R\beta}}\gamma_\mu u_{R\beta})+\cdots+(\overline{b_{R\beta}}\gamma_\mu b_{R\beta})],\\
O_6&=(\overline{s_{L\alpha}}\gamma^\mu b_{L\beta})[(\overline{u_{R\beta}}\gamma_\mu u_{R\alpha})+\cdots+(\overline{b_{R\beta}}\gamma_\mu b_{R\alpha})],\\
O_7&=(e/16\pi^2)\overline{s_\alpha}\sigma^{\mu\nu}[m_b(\mu)R+m_s(\mu)L]b_\alpha F_{\mu\nu},\\
O_8&=(g_s/16\pi^2)\overline{s_\alpha}\sigma^{\mu\nu}[m_b(\mu)R+m_s(\mu)L](\lambda^A_{\alpha\beta}/2)b_\beta G^A_{\mu\nu}.
\end{aligned} \qquad (1.2)$$

In the dipole-type operators O_7 and O_8, e and $F_{\mu\nu}$ (g_s and $G^A_{\mu\nu}$) denote the electromagnetic (strong) coupling constant and field strength tensor, respectively. $L=(1-\gamma_5)/2$ and $R=(1+\gamma_5)/2$ stand for the left- and right-handed projection operators. It should be stressed in this context that the explicit mass factors in O_7 and O_8 are the running quark masses.

QCD corrections to the decay rate for $b\to s\gamma$ bring in large logarithms of the form $\alpha_s^n(m_W)\ln^m(m_b/M)$, where

*Present address: ITP, SUNY at Stony Brook, Stony Brook, NY 11794-3840.

[1]Some of the diagrams were calculated by Soares [8].

TABLE I. Leading logarithmic Wilson coefficients $C_i(\mu)$ at the matching scale $\mu=m_W=80.33$ GeV and at three other scales, $\mu=10.0$ GeV, $\mu=5.0$ GeV, and $\mu=2.5$ GeV. For $\alpha_s(\mu)$ (in the $\overline{\text{MS}}$ scheme) we used the one-loop expression with five flavors and $\alpha_s(m_Z)=0.117$. The entries correspond to the top quark mass $\overline{m_t}(m_{t,\text{pole}})=170$ GeV (equivalent to $m_{t,\text{pole}}=180$ GeV).

$C_i(\mu)$	$\mu=m_W$	$\mu=10.0$ GeV	$\mu=5.0$ GeV	$\mu=2.5$ GeV
C_1	0.0	−0.149	−0.218	−0.305
C_2	1.0	1.059	1.092	1.138
C_3	0.0	0.006	0.010	0.014
C_4	0.0	−0.016	−0.023	−0.031
C_5	0.0	0.005	0.007	0.009
C_6	0.0	−0.018	−0.027	−0.040
C_7	−0.192	−0.285	−0.324	−0.371
C_8	−0.096	−0.136	−0.150	−0.166
C_7^{eff}	−0.192	−0.268	−0.299	−0.334
C_8^{eff}	−0.096	−0.131	−0.143	−0.157

$M=m_t$ or m_W and $m\leqslant n$ (with $n=0,1,2,\ldots$). One can systematically resum these large terms by renormalization group techniques. Usually, one matches the full standard model theory with the effective theory at the scale m_W. At this scale, the large logarithms generated by matrix elements in the effective theory are the same ones as in the full theory. Consequently, the Wilson coefficients only contain small QCD corrections. Using the renormalization group equation, the Wilson coefficients are then calculated at the scale $\mu\approx m_b$, the relevant scale for a B meson decay. At this scale the large logarithms are contained in the Wilson coefficients while the matrix elements of the operators are free of them.

As noted, so far the decay rate for $b\to s\gamma$ has been systematically calculated only to leading logarithmic accuracy, i.e., $m=n$. To this precision it is consistent to perform the ''matching'' of the effective and full theory without taking into account QCD corrections [10] and to calculate the anomalous dimension matrix to order α_s [11]. The corresponding leading logarithmic Wilson coefficients are given explicitly in [6,12]. Their numerical values in the naive dimensional regularization (NDR) scheme are listed in Table I for different values of the renormalization scale μ. The leading logarithmic contribution to the decay matrix element is then obtained by calculating the tree-level matrix element of the operator C_7O_7 and the one-loop matrix elements of the four-Fermi operators C_iO_i $(i=1,\ldots,6)$. In the NDR scheme the latter can be absorbed into a redefinition[2] of $C_7\to C_7^{\text{eff}}$:

$$C_7^{\text{eff}}\equiv C_7+Q_dC_5+3Q_dC_6. \tag{1.3}$$

In the 't Hooft–Veltman scheme (HV) [13], the contribution of the four-Fermi operators vanishes. The Wilson coefficients C_7 and C_8 in the HV scheme are identical to C_7^{eff} and C_8^{eff} in the NDR scheme. Consequently, the complete leading logarithmic result for the decay amplitude $b\to s\gamma$ is indeed scheme independent.

Since the first order calculations have large scale uncertainties, it is important to take into account the next-to-leading order corrections. They are most prominent in the photon energy spectrum. While it is a δ function (which is smeared out by the Fermi motion of the b quark inside the B meson) in the leading order, bremsstrahlung corrections, i.e., the process $b\to s\gamma g$, broaden the shape of the spectrum substantially. Therefore, these important corrections have been taken into account for the contributions of the operators O_7 and O_2 some time ago [3] and recently also of the full operator basis [4,14,15]. As expected, the contributions of O_7 and O_2 are by far the most important ones, especially in the experimentally accessible part of the spectrum. Also, those (next-to-leading) corrections, which are necessary to cancel the infrared (and collinear) singularities of the bremsstrahlung diagrams, were included. These are the virtual gluon corrections to the contribution of the operator O_7 for $b\to s\gamma$ and the virtual photon corrections to O_8 for $b\to sg$.

A complete next-to-leading calculation implies two classes of improvements: First, the Wilson coefficients to next leading order at the scale $\mu\approx m_b$ are required. To this end the matching with the full theory (at $\mu=m_W$) must be done at the $O(\alpha_s)$ level and the renormalization group equation has to be solved using the anomalous dimension matrix calculated up to order α_s^2. Second, the virtual $O(\alpha_s)$ corrections for the matrix element (at scale $\mu\approx m_b$) must be evaluated and combined with the bremsstrahlung corrections. The higher order matching has been calculated in Ref. [16] and work on the Wilson coefficients is in progress. In this paper we will evaluate all the virtual corrections beyond those already evaluated in connection with the bremsstrahlung process. We expect them to reduce substantially the strong scale dependence of the leading order calculation.

Among the four-Fermi operators, only O_2 contributes sizably and we calculate only its virtual corrections to the matrix element for $b\to s\gamma$. The matrix element O_1 vanishes because of color, and the penguin-induced four-Fermi operators $O_3,\ldots,O_6$ can be neglected[3] because their Wilson coefficients[4] are much smaller than C_2, as illustrated in Table I. However, we do take into account the virtual $O(\alpha_s)$ corrections to $b\to s\gamma$ associated with the magnetic operators O_7 (which has already been calculated in the literature) and O_8 (which is new). Since the corrections to O_7 and O_8 are one-loop diagrams, they are relatively easy to work out. In contrast, the corrections to O_2 involve two-loop diagrams, since this operator itself only contributes at the one-loop level.

Since the virtual and bremsstrahlung corrections to the matrix elements are only one (well-defined) part of the whole next-to-leading program, we expect that this contribution alone will depend on the renormalization scheme used. Even within the modified minimal subtraction scheme ($\overline{\text{MS}}$) used here, we expect that two different ''prescriptions'' how to treat γ_5 will lead to different answers. Since previous calcu-

[2]For the analogous $b\to sg$ transition, the effects of the four-Fermi operators can be absorbed by the shift $C_8\to C_8^{\text{eff}}=C_8+C_5$.

[3]This omission will be a source of a slight scheme and scale dependence of the next-to-leading order result.

[4]It is consistent to calculate the corrections using the leading logarithmic Wilson coefficients.

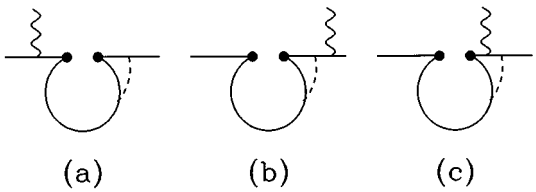

FIG. 1. Diagrams 1(a), 1(b), and 1(c) associated with the operator O_2. The fermions (b, s, and c quark) are represented by solid lines. The wavy (dashed) line represents the photon (gluon).

lations of the bremsstrahlung diagrams have been done in the NDR scheme and also the leading logarithmic Wilson coefficients are available in this scheme, we also use it here. For future checks, however, we also consider in Appendix A the corresponding calculation in the HV scheme.

The remainder of this paper is organized as follows. In Sec. II we give the two-loop corrections for $b\to s\gamma$ based on the operator O_2 together with the counterterm contributions. In Sec. III the virtual corrections for $b\to s\gamma$ based on O_7 are reviewed including some of the bremsstrahlung corrections. Then, in Sec. IV we calculate the one-loop corrections to $b\to s\gamma$ associated with O_8. Section V contains the results for the branching ratio for $b\to s\gamma(g)$ and especially the drastic reduction of the renormalization scale dependence due to the new contributions. Appendix A contains the result of the O_2 two-loop calculation in the HV scheme and, finally, to make the paper self-contained, we include in Appendix B the bremsstrahlung corrections to the operators O_2, O_7, and O_8.

II. VIRTUAL CORRECTIONS TO O_2 IN THE NDR SCHEME

In this section we present the calculation of the matrix element of the operator O_2 for $b\to s\gamma$ up to order α_s in the NDR scheme. The one-loop (α_s^0) matrix element vanishes and we must consider several two-loop contributions. Since they involve ultraviolet singularities also, counterterm contributions are needed. These are easy to obtain because the operator renormalization constants Z_{ij} are known with enough accuracy from the order α_s anomalous dimension matrix [11]. Explicitly, we need the contributions of the operators $C_2\delta Z_{2j}O_j$ to the matrix element for $b\to s\gamma$, where δZ_{2j} denote the order α_s contribution of the operator renormalization constants. In the NDR scheme, the nonvanishing counterterms come from the one-loop matrix element of $C_2\delta Z_{25}O_5$ and $C_2\delta Z_{26}O_6$ as well as from the tree-level matrix element of the operator $C_2\delta Z_{27}O_7$. We also note that there are no contributions to $b\to s\gamma$ from counterterms proportional to evanescent operators multiplying the Wilson coefficient C_2.

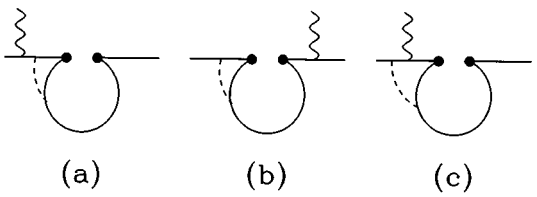

FIG. 2. Diagrams 2(a), 2(b), and 2(c) associated with the operator O_2.

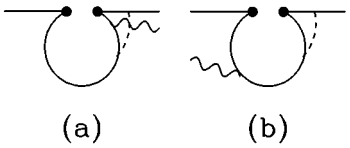

FIG. 3. Diagrams 3(a) and 3(b) associated with the operator O_2. We calculate directly their sum and denote it by $M_2(3)$, see text.

A. Regularized two-loop contribution of O_2

The dimensionally regularized matrix element M_2 of the operator O_2 for $b\to s\gamma$

$$M_2=\langle s\gamma|O_2|b\rangle \tag{2.1}$$

can be divided into four classes of nonvanishing two-loop diagrams, as shown in Figs. 1–4. The sum of the diagrams in each class (=figure) is gauge invariant. The contributions to the matrix element M_2 of the individual classes (Figs.) 1–4 are denoted by $M_2(1),M_2(2),M_2(3)$, and $M_2(4)$, where, e.g., $M_2(1)$ is

$$M_2(1)\equiv M_2(1a)+M_2(1b)+M_2(1c). \tag{2.2}$$

The main steps of the calculation are the following: We first calculate the Fermion loops in the individual diagrams, i.e., the ''building blocks'' shown in Figs. 5 and 6, combining together the two diagrams in Fig. 6. As usual, we work in $d=4-2\epsilon$ dimensions; the results are presented as integrals over Feynman parameters after integrating over the (shifted) loop momentum. Then, we insert these building blocks into the full two-loop diagrams. Using the Feynman parametrization again, we calculate the integral over the second loop momentum. As the remaining Feynman parameter integrals contain rather complicated denominators, we do not evaluate them directly. At this level we also do not expand in the regulator ϵ. The heart of our procedure which will be explained more explicitly below, is to represent these denominators as complex Mellin-Barnes integrals [17]. After inserting this representation and interchanging the order of integration, the Feynman parameter integrals are reduced to well-known Euler β functions. Finally, the residue theorem allows to write the result of the remaining complex integal as the sum over the residues taken at the pole positions of certain β and Gamma functions; this naturally leads to an expansion in the ratio $z=(m_c/m_b)^2$, which numerically is about $z=0.1$.

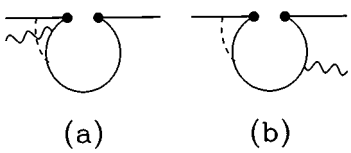

FIG. 4. Diagrams 4(a) and 4(b) associated with the operator O_2. We calculate directly their sum and denote it by $M_2(4)$, see text.

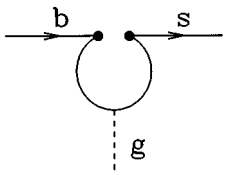

FIG. 5. Building block I_β for the diagrams in Figs. 1 and 2 with an off-shell gluon.

We express the diagram in Fig. 5 (denoted by I_β) in a way convenient for inserting into the two-loop diagrams. As we will use $\overline{\text{MS}}$ subtraction later on, we introduce the renormalization scale in the form $\mu^2\exp(\gamma_E)/(4\pi)$, where $\gamma_E=0.577\ldots$ is the Euler constant. Then, $\overline{\text{MS}}$ corresponds to subtracting the poles in ϵ. In the NDR scheme, I_β is given by[5]

$$I_\beta=-\frac{g_s}{4\pi^2}\Gamma(\epsilon)\mu^{2\epsilon}\exp(\gamma_E\epsilon)(1-\epsilon)\exp(i\pi\epsilon)(r_\beta \not{r} - r^2\gamma_\beta)L\frac{\lambda}{2}\int_0^1[x(1-x)]^{1-\epsilon}\left[r^2-\frac{m_c^2}{x(1-x)}+i\delta\right]^{-\epsilon}, \tag{2.3}$$

where r is the four-momentum of the (off-shell) gluon, m_c is the mass of the charm quark propagating in the loop and the term $i\delta$ is the ''ϵ prescription.'' The free index β will be contracted with the gluon propagator when inserting the building block into the two-loop diagrams in Figs. 1 and 2. Note that I_β is gauge invariant in the sense that $r^\beta I_\beta=0$.

Next, we give the sum of the two diagrams in Fig. 6, using the decomposition in [18]. We get (denoting this building block by $J_{\alpha\beta}$)

$$J_{\alpha\beta}=\frac{eg_sQ_u}{16\pi^2}\left[E(\alpha,\beta,r)\Delta i_5+E(\alpha,\beta,q)\Delta i_6-E(\beta,r,q)\frac{r_\alpha}{(qr)}\Delta i_{23}-E(\alpha,r,q)\frac{r_\beta}{(qr)}\Delta i_{25}-E(\alpha,r,q)\frac{q_\beta}{(qr)}\Delta i_{26}\right]L\frac{\lambda}{2}, \tag{2.4}$$

where q is the four-momentum of the photon. The index α in Eq. (2.4) is understood to be contracted with the polarization vector ε of the photon, while the index β is contracted with the gluon propagator in the two-loop diagrams in Figs. 3 and 4. The matrix E in Eq. (2.4) is defined as

$$E(\alpha,\beta,r)=\gamma_\alpha\gamma_\beta\not{r}-\gamma_\alpha r_\beta+\gamma_\beta(r_\alpha)-\not{r}g_{\alpha\beta}. \tag{2.5}$$

In a four-dimensional context these E quantities can be reduced to expressions involving the Levi-Cività tensor, i.e., $E(\alpha,\beta,\gamma)=-i\varepsilon_{\alpha\beta\gamma\mu}\gamma^\mu\gamma_5$ (in the Bjorken-Drell convention). The dimensionally regularized expressions for the Δi read

[5]The fermion-gluon and the fermion-photon couplings are defined according to the covariant derivative $D=\partial+ig_s(\lambda^B/2)A^B+ieQA$.

FIG. 6. Building block $J_{\alpha\beta}$ for the diagrams in Figs. 3 and 4.

$$\Delta i_5=-4\int_S dxdy[4(qr)x^2y\epsilon-4(qr)xy\epsilon-2r^2x^3\epsilon+3r^2x^2\epsilon-r^2x\epsilon+3xC-C][(1+\epsilon)\Gamma(\epsilon)\times\exp(\gamma_E\epsilon)\mu^{2\epsilon}C^{-1-\epsilon}], \tag{2.6}$$

$$\Delta i_6=4\int_S dxdy[4(qr)xy^2\epsilon-4(qr)xy\epsilon-2r^2x^2y\epsilon+2r^2x^2\epsilon+r^2xy\epsilon-2r^2x\epsilon+3yC-C][(1+\epsilon)\Gamma(\epsilon)\times\exp(\gamma_E\epsilon)\mu^{2\epsilon}C^{-1-\epsilon}], \tag{2.7}$$

$$\Delta i_{23}=-\Delta i_{26}=8(qr)\int_S dxdy[xy\epsilon(1+\epsilon)\Gamma(\epsilon)\times\exp(\gamma_E\epsilon)\mu^{2\epsilon}C^{-1-\epsilon}], \tag{2.8}$$

$$\Delta i_{25}=-8(qr)\int_S dxdy[x(1-x)\epsilon(1+\epsilon)\Gamma(\epsilon)\times\exp(\gamma_E\epsilon)\mu^{2\epsilon}C^{-1-\epsilon}], \tag{2.9}$$

where C and $C^{-1-\epsilon}$ are given by

$$C=m_c^2-2xy(qr)-x(1-x)r^2-i\delta,$$

$$C^{-1-\epsilon}=-\exp(i\pi\epsilon)[x(1-x)]^{-1-\epsilon}\times\left[r^2+\frac{2y(qr)}{1-x}-\frac{m_c^2}{x(1-x)}+i\delta\right]^{-1-\epsilon}. \tag{2.10}$$

The range of integration in (x,y) is restricted to the simplex S, i.e., $0\leq y\leq(1-x)$ and $0\leq x\leq 1$.

Due to Ward identities, not all the Δi are independent. The identities given in Ref. [18] in the context of the full theory simplify in our case as follows:

$$q^\alpha J_{\alpha\beta}=0, \quad r^\beta J_{\alpha\beta}=0. \tag{2.11}$$

They allow us to express Δi_5 and Δi_6 in terms of the other Δi which have a more compact form. These relations read

$$\Delta i_5=\Delta i_{23},$$

$$\Delta i_6=\frac{r^2}{(qr)}\Delta i_{25}+\Delta i_{26}. \tag{2.12}$$

Of course, Eq. (2.12) can be checked explicitly for all values of ϵ, using partial integration and certain symmetry properties of the integrand.

We are now ready to evaluate the two-loop diagrams. As both I_β and $J_{\alpha\beta}$ are transverse with respect to the gluon, the gauge of the gluon propagator is irrelevant. Also, due to the

absence of extra singularities in the limit of vanishing strange quark mass, we set $m_s=0$ from the very beginning (the question of charm quark mass ''singularities'' will be discussed later).

As an example, we present the calculation of the two-loop diagram in Fig. 1(c) in some detail. Using I_β in Eq. (2.3), the matrix element reads

$$\begin{aligned} M[\text{Fig. 1}(c)] = & \frac{i}{4\pi^2} e Q_d g_s^2 C_F \Gamma(\epsilon) \exp(2\gamma_E \epsilon) \mu^{4\epsilon} \\ & \times (1-\epsilon)\exp(i\pi\epsilon) \\ & \times (4\pi)^{-\epsilon} \int \frac{d^d r}{(2\pi)^d} \overline{u}(p') \gamma^\beta \frac{\not p' - \not r}{(p'-r)^2} \not\epsilon \\ & \times \frac{\not p - \not r}{(p-r)^2} (r_\beta \not r - r^2 \gamma_\beta) L u(p) \frac{1}{r^2} \\ & \times \int_0^1 dx \frac{[x(1-x)]^{1-\epsilon}}{\{r^2 - m_c^2/[x(1-x)] + i\delta\}^\epsilon}. \end{aligned} \tag{2.13}$$

In Eq. (2.13), $u(p')$ and $u(p)$ are the Dirac spinors for the s and the b quarks, respectively, and $C_F=4/3$. In the next step, the four propagator factors in the denominator are Feynman parametrized as

$$\begin{aligned} \frac{1}{D_1 D_2 D_3 D_4^\epsilon} = & \frac{\Gamma(3+\epsilon)}{\Gamma(\epsilon)} \\ & \times \int \frac{du\,dv\,dw\,dy\, y^{\epsilon-1} \delta(1-u-v-w-y)}{[D_1 u + D_2 v + D_3 w + D_4 y]^{3+\epsilon}}, \end{aligned} \tag{2.14}$$

where $D_1=(p'-r)^2$, $D_2=(p-r)^2$, $D_3=r^2$, and $D_4=r^2-m_c^2/[x(1-x)]$. Then, the integral over the loop momentum r is performed. Making use of the δ function in Eq. (2.14), the integral over w is easy. The remaining variables u, v, and y are transformed into new variables u', v', and y', all of them varying in the interval [0,1]. The substitution reads

$$u \to v'(1-u'), \quad v \to v'u', \quad y \to (1-v')y'. \tag{2.15}$$

Taking into account the corresponding Jacobian and omitting the primes($'$) of the integration variables this leads to

$$\begin{aligned} M[\text{Fig. 1(c)}] = & \frac{1}{64\pi^4} e Q_d g_s^2 C_F \Gamma(2\epsilon) \exp(2\gamma_E \epsilon) \mu^{4\epsilon} \\ & \times \exp(2i\pi\epsilon)(1-\epsilon) \int dx\,du\,dv\,dy \\ & \times [x(1-x)]^{1-\epsilon} y^{\epsilon-1} (1-v)^\epsilon v \overline{u}(p') \\ & \times \left[P_1 \frac{\hat{C}}{\hat{C}^{2\epsilon}} + P_2 \frac{1}{\hat{C}^{2\epsilon}} + P_3 \frac{1}{\hat{C}^{1+2\epsilon}} \right] u(p), \end{aligned} \tag{2.16}$$

where P_1, P_2, and P_3 are matrices in Dirac space depending on the Feynman parameters x, u, v, y in a polynomial way. $\hat{C}$ is given by

$$\hat{C} = m_b^2 v(1-v)u - \frac{m_c^2}{x(1-x)}(1-v)y + i\delta. \tag{2.17}$$

In what follows, the ultraviolet ϵ regulator remains a fixed, small positive number.

The central point of our procedure is to use now the Mellin-Barnes representation of the ''propagator'' $1/(k^2-M^2)^\lambda$ [19–22] which is given by

$$\begin{aligned} \frac{1}{(k^2-M^2)^\lambda} = & \frac{1}{(k^2)^\lambda \Gamma(\lambda)} \frac{1}{2\pi i} \int_\gamma ds (-M^2/k^2)^s \Gamma(-s) \\ & \times \Gamma(\lambda+s), \end{aligned} \tag{2.18}$$

where $\lambda>0$ and γ denotes the integration path which is parallel to the imaginary axis (in the complex s plane) hitting the real axis somewhere between $-\lambda$ and 0. In this formula, the ''momentum squared'' k^2 is understood to have a small positive imaginary part. In Refs. [19,21] exact solutions to Feynman integrals containing massive propagators are obtained by representing their denominators according to the formula (2.18) with subsequent calculation of the corresponding massless integrals.

In our approach, we use formula (2.18) in order to simplify the remaining Feynman parameter integrals in Eq. (2.16). We represent the factors $1/\hat{C}^{2\epsilon}$ and $1/\hat{C}^{1+2\epsilon}$ in Eq. (2.16) as Mellin-Barnes integrals using the identifications

$$k^2 \leftrightarrow m_b^2 v(1-v)u; \quad M^2 \leftrightarrow \frac{m_c^2}{x(1-x)}(1-v)y. \tag{2.19}$$

By interchanging the order of integration, we first carry out the integrals over the Feynman parameters for any given fixed value of s on the integration path γ. These integrals are basically the same as for the massless case $m_c=0$ [in Eqs. (2.16) and (2.17)] up to a factor (in the integrand) of

$$\left[\frac{y}{uvx(1-x)} \right]^s \exp(i\pi s) \left(\frac{m_c^2}{m_b^2} \right)^s. \tag{2.20}$$

Note that the polynomials P_1, P_2, and P_3 have such a form that the Feynman parameter integrals exist in the limit $m_c \to 0$. If the integration path γ is chosen close enough to the imaginary axis, the factor in Eq. (2.20) does not change the convergence properties of the integrals, i.e., the Feynman parameter integrals exist for all values of s lying on γ. It is easy to see that the only integrals involved are of the type

$$\begin{aligned} \int_0^1 dw w^p \quad \text{or} \quad \int_0^1 dw w^p (1-w)^q &= \beta(p+1,q+1) \\ &= \frac{\Gamma(p+1)\Gamma(q+1)}{\Gamma(p+q+2)}. \end{aligned} \tag{2.21}$$

For the s integration we use the residue theorem after closing the integration path in the right s-half plane. One has to show that the integral over the half circle vanishes if its radius goes to ∞. As we explicitly checked, this is indeed the case for

$(m_c^2/m_b^2)<1/4$, which is certainly satisfied in our application. The poles which lie inside the integration contour are located at

$$s=0,1,2,3,4,\ldots,$$

$$s=1-\epsilon,\quad 2-\epsilon,\quad 3-\epsilon,\quad 4-\epsilon,\ldots,$$

$$s=1-2\epsilon,\quad 2-2\epsilon,\quad 3-2\epsilon,\quad 4-2\epsilon,\ldots. \tag{2.22}$$

The other two-loop diagrams are evaluated similarly. The nontrivial Feynman integrals can always be reduced to those given in Eq. (2.21) after some suitable substitutions. The only change is that there are poles in addition to those given in Eq. (2.22) in those diagrams where the gluon hits the b-quark line; they are located at

$$s=1/2-2\epsilon,\quad s=3/2-2\epsilon,\quad s=5/2-2\epsilon,$$

$$s=7/2-2\epsilon,\ldots. \tag{2.23}$$

The sum over the residues naturally leads to an expansion in $z=(m_c^2/m_b^2)$ through the factor $(m_c^2/m_b^2)^s$ in Eq. (2.20). This expansion, however, is not a Taylor series because it also involves logarithms of z, which are generated by the expansion in ϵ. A generic diagram which we denote by G has, then, the form

$$G=c_0+\sum_{n,m} c_{nm} z^n \ln^m z,\quad z=\frac{m_c^2}{m_b^2}, \tag{2.24}$$

where the coefficients c_0 and c_{nm} are independent of z. The power n in Eq. (2.24) is, in general, a natural multiple of 1/2 and m is a natural number including 0. In the explicit calculation, the lowest n turns out to be $n=1$. This implies the important fact that the limit $m_c\to 0$ exists; thus, there cannot be large logarithms (from a small up-quark mass) in these diagrams.

From the structure of the poles one can see that the power m of the logarithm is bounded by four, independent of the value of n. To illustrate this, take $n=100$ as an example. There are three poles located near $n=100$, viz., at $s=100$, $s=100-\epsilon$, $s=100-2\epsilon$, respectively [see Eq. (2.22)]. Taking the residue at one of them, yields a term proportional to $1/\epsilon^2$ coming from the remaining two poles. In addition, there can be an explicit $1/\epsilon^2$ term from the integration of the two-loop momenta. Therefore, the most singular term can be $1/\epsilon^4$. Multiplying this with z^s in Eq. (2.20) leads to $z^{100}\ln^m z$ where m can be four at most.

We have retained all terms up to $n=3$. Comparing the $n=3$ numerical result with the one obtained by truncating at $n=2$ leads to a difference of about 1% only.

We have made further checks of our procedure. For example, we have calculated diagram 1(b) directly. Expanding the result, we reproduce the expressions obtained by applying the Mellin-Barnes integral at the Feynman parameter level as described above. A similar exercise for the imaginary part of diagram 1(c) shows that the exact and the expanded result (up to z^3 terms) in these examples agree at the 1% level. In addition, we checked that the imaginary part of the sum of all diagrams coincides numerically with the results of Soares [23,8] (note, however, that in the physical region only the diagrams in Figs. 1 and 3 contribute to the imaginary part). In Ref. [8], Soares applied dispersion techniques to calculate the real part. However, using the imaginary part in the physical region, only the real part of the diagrams in Figs. 1 and 3 is obtained. We have checked that our numbers for these two sets of diagrams indeed coincide with the results of Soares. However, the contribution of the diagrams in Figs. 2 and 4 is missing in [8] because the additional unphysical cuts were not taken into account. We also note that a separate consideration of the subtraction terms would be required to obtain the correct μ dependence.

We mention that the Dirac algebra has been done with the algebraic program REDUCE[6] [24]. The Feynman parameter integrals and the determination of the residues have been done with the symbolic program MAPLE [26].

We now give the results for the diagrams shown in Figs. 1–4. As already mentioned, the individual diagrams in each figure are not gauge invariant but only their sum is. Note that the leading ultraviolet singularity in the individual two-loop diagrams is, in general, of order $1/\epsilon^2$. In the gauge-invariant sums $M_2(i)$, the $1/\epsilon^2$ cancel and we are left with $1/\epsilon$ poles only. The results read [using $z=(m_c/m_b)^2$ and $L=\ln z$]

$$\begin{aligned} M_2(1)=\Bigg\{ & \frac{1}{36\epsilon}\left(\frac{m_b}{\mu}\right)^{-4\epsilon}+\frac{1}{216}[37-(540+216L)z \\ & +(216\pi^2-540+216L-216L^2)z^2 \\ & -(144\pi^2+136+240L-144L^2)z^3] \\ & +\frac{i\pi}{18}[1-18z+(18-36L)z^2+(24L-20)z^3]\Bigg\} \\ & \times\frac{\alpha_s}{\pi}C_F Q_d\langle s\gamma|O_7|b\rangle_{\rm tree}, \end{aligned} \tag{2.25}$$

$$\begin{aligned} M_2(2)=\Bigg\{ & -\frac{5}{36\epsilon}\left(\frac{m_b}{\mu}\right)^{-4\epsilon}+\frac{1}{216}[13+(36\pi^2-108)z \\ & -144\pi^2 z^{3/2}+(648-648L+108L^2)z^2 \\ & +(120\pi^2-314+12L+288L^2)z^3]\Bigg\} \\ & \frac{\alpha_s}{\pi}C_F Q_d\langle s\gamma|O_7|b\rangle_{\rm tree}, \end{aligned} \tag{2.26}$$

[6]Some checks have been done with TRACER [25].

$$M_2(3)=\Bigg\{-\frac{1}{8\epsilon}\left(\frac{m_b}{\mu}\right)^{-4\epsilon}+\frac{1}{48}\{-45+[72-12\pi^2-96\zeta(3)+(96-24\pi^2)L+12L^2+8L^3]z+[60+24\pi^2-96\zeta(3)+(24-24\pi^2)L-24L^2+8L^3]z^2-(68-48L)z^3\}+\frac{i\pi}{12}[-3+(24-2\pi^2+6L+6L^2)z+(6-2\pi^2-12L+6L^2)z^2+12z^3]\Bigg\}\times\frac{\alpha_s}{\pi}C_F Q_u\langle s\gamma|O_7|b\rangle_{\rm tree}, \tag{2.27}$$

$$M_2(4)=\Bigg\{-\frac{1}{4\epsilon}\left(\frac{m_b}{\mu}\right)^{-4\epsilon}-\frac{1}{24}\{21+[-24+2\pi^2+24\zeta(3)-(12-6\pi^2)L+2L^3]z+[-12-4\pi^2-48\zeta(3)+12L-6L^2+2L^3]z^2+(-6+6\pi^2-24L+18L^2)z^3\}\Bigg\}\times\frac{\alpha_s}{\pi}C_F Q_u\langle s\gamma|O_7|b\rangle_{\rm tree}. \tag{2.28}$$

In these expressions, the symbol ζ denotes the Riemann ζ function, with $\zeta(3)\approx 1.2021$; $Q_u=2/3$ and $Q_d=-1/3$ are the charge factors for up- and down-type quarks, respectively. The matrix element $\langle s\gamma|O_7|b\rangle_{\rm tree}$ is the $O(\alpha_s^0)$ tree-level matrix element of the operator O_7; its explicit form is

$$\langle s\gamma|O_7|b\rangle_{\rm tree}=m_b\frac{e}{8\pi^2}\overline{u}(p')\not{\epsilon}\not{q}Ru(p). \tag{2.29}$$

In formula (2.29) m_b should be identified with the running mass $m_b(\mu)$ in principle [see Eq. (1.2)]. However, as the corrections to O_2 are explicitly proportional to α_s, m_b can be identified with the pole mass as well [apart from $O(\alpha_s^2)$ corrections which we systematically neglect].

B. Counterterms

The operators mix under renormalization and thus the counterterm contributions must be taken into account. As we are interested in this section in contributions to $b\to s\gamma$ which are proportional to C_2, we have to include, in addition to the two-loop matrix elements of C_2O_2, also the one-loop matrix elements of the four-Fermi operators $C_2\delta Z_{2j}O_j$ ($j=1,\ldots,6$) and the tree-level contribution of the magnetic operator $C_2\delta Z_{27}O_7$. In the NDR scheme the only nonvanishing contributions to $b\to s\gamma$ come from $j=5,6,7$. (For $j=5,6$ the contribution comes from the diagram in which the internal b quark emits the photon.) The operator renormalization constants Z_{ij} are listed in the literature [11] in the context of the leading order anomalous dimension matrix. The entries needed in our calculation are

$$\delta Z_{25}=-\frac{\alpha_s}{48\pi\epsilon}C_F,\quad \delta Z_{26}=\frac{\alpha_s}{16\pi\epsilon}C_F,$$

$$\delta Z_{27}=\frac{\alpha_s}{16\pi\epsilon}\left(6Q_u-\frac{8}{9}Q_d\right)C_F. \tag{2.30}$$

Defining

$$M_{2j}=\langle s\gamma|\delta Z_{2j}O_j|b\rangle, \tag{2.31}$$

we find the following contributions to the matrix elements

$$M_{25}=-\frac{\alpha_s}{48\pi}Q_dC_F\frac{1}{\epsilon}\left(\frac{m_b}{\mu}\right)^{-2\epsilon}\langle s\gamma|O_7|b\rangle_{\rm tree},$$

$$M_{26}=\frac{3\alpha_s}{16\pi}Q_dC_F\frac{1}{\epsilon}\left(\frac{m_b}{\mu}\right)^{-2\epsilon}\langle s\gamma|O_7|b\rangle_{\rm tree},$$

$$M_{27}=\frac{\alpha_s}{\pi}\left(\frac{3Q_uC_F}{8}-\frac{Q_dC_F}{18}\right)\frac{1}{\epsilon}\langle s\gamma|O_7|b\rangle_{\rm tree}. \tag{2.32}$$

We note that there is no one-loop contribution to the matrix element for $b\to s\gamma$ from the counterterm proportional to $C_2(1/\epsilon)O_{12}^{\rm ev}$ where the evanescent operator $O_{12}^{\rm ev}$ (see, e.g., the last Ref. in [11]) reads

$$O_{12}^{\rm ev}=\frac{1}{6}O_2(\gamma_\mu\to\gamma_{[\mu}\gamma_\nu\gamma_{\rho]})-O_2. \tag{2.33}$$

C. Renormalized contribution proportional to C_2

Adding the two-loop diagrams from Sec. 2 A [Eqs. (2.25)–(2.28)] and the counterterms from Sec. 2 B [Eq. (2.32)], we find the renormalized contribution M_2:

$$M_2=M_2(1)+M_2(2)+M_2(3)+M_2(4)+M_{25}+M_{26}+M_{27}. \tag{2.34}$$

Of course, the ultraviolet singularities cancel in M_2. Inserting $C_F=4/3$, $Q_u=2/3$, and $Q_d=-1/3$, we get the main result of this paper, which in the NDR scheme reads

$$M_2=\langle s\gamma|O_7|b\rangle_{\rm tree}\frac{\alpha_s}{4\pi}\left(\mathscr{C}_2\ln\frac{m_b}{\mu}+r_2\right), \tag{2.35}$$

with

$$\mathscr{C}_2=\frac{416}{81}, \tag{2.36}$$

$$\mathrm{Re}r_2=\frac{2}{243}\{-833+144\pi^2z^{3/2}+[1728-180\pi^2-1296\zeta(3)+(1296-324\pi^2)L+108L^2+36L^3]z+[648+72\pi^2+(432-216\pi^2)L+36L^3]z^2+[-54-84\pi^2+1092L-756L^2]z^3\}, \tag{2.37}$$

$$\mathrm{Im}r_2=\frac{16\pi}{81}\{-5+[45-3\pi^2+9L+9L^2]z+[-3\pi^2+9L^2]z^2+[28-12L]z^3\}. \tag{2.38}$$

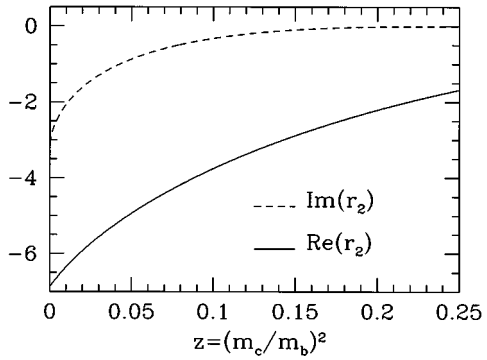

FIG. 7. Real and imginary part of r_2 in the NDR scheme [from Eqs. (2.37) and (2.38)].

Here, Rer_2 and Imr_2 denote the real and the imaginary part of r_2, respectively. The quantity z is defined as $z=(m_c^2/m_b^2)$ and $L=\ln(z)$. In Fig. 7 we show the real and the imaginary part of r_2. For $z\geqslant 1/4$ the imaginary part must vanish exactly; indeed, we see from Fig. 7 that the imaginary part based on the expansion retaining terms up to z^3 indeed vanishes at $z=1/4$ to high accuracy.

III. $O(\alpha_s)$ CORRECTIONS TO O_7

The virtual corrections associated with the operator O_7 as shown in Fig. 8(b) (together with the self-energy diagrams and the counterterms) have been taken into account in the work of Ali and Greub, see, e.g. [3,4,14], where $m_s\neq 0$ was retained. Since we neglect m_s in this work, we are interested only in the limit $m_s\to 0$. Because of the mass singularities in the virtual corrections (which will be canceled when also taking into account bremsstrahlung corrections), we only keep m_s as a regulator.

Including the lowest order contribution, the result then becomes [using $\rho=(m_s/m_b)^2$] in the NDR scheme

$$\langle s\gamma|O_7|b\rangle_{\rm virt}=\langle s\gamma|O_7|b\rangle_{\rm tree}[1+\hat{K}_g], \tag{3.1}$$

$$\hat{K}_g=\frac{\alpha_s}{6\pi}\left(\frac{4\pi\mu^2}{m_b^2}\right)^{\epsilon_{\rm IR}}\Gamma(1+\epsilon_{\rm IR}) \times\left\{\ln^2\rho-\frac{2}{\epsilon_{IR}}\ln\rho-\ln\rho-\frac{4}{\epsilon_{IR}}-8+4\ln\frac{m_b}{\mu}\right\}. \tag{3.2}$$

Note that Eq. (3.1) contains all the counterterm contributions. The $1/\epsilon_{\rm IR}$ poles in this equation are, therefore, of infrared origin as indicated by the notation. The last term in the curly bracket in Eq. (3.2) represents a μ dependence of ultraviolet origin. The additional μ dependence, which is generated when expanding in $\epsilon_{\rm IR}$ is canceled at the level of the decay width together with the $1/\epsilon_{\rm IR}$ poles when adding the bremsstrahlung correction due to the square of the diagrams associated with the operator O_7. As all intermediate formulas are given in the literature, we only give the final result for the α_s corrections (virtual+bremsstrahlung) to the decay width. Denoting this contribution by Γ_{77} we get, in the limit $m_s=0$,

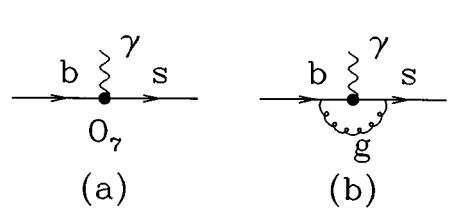

FIG. 8. Virtual corrections to O_7.

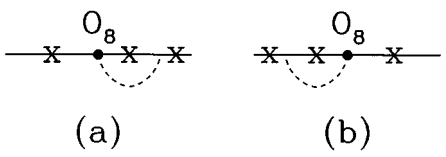

FIG. 9. Contributions of O_8 to $b\to s\gamma$. The cross (x) denotes the possible place where the photon is emitted. Figures 9(a) and 9(b) are separately gauge invariant.

$$\Gamma_{77}=\Gamma_{77}^0\left[1+\frac{\alpha_s}{3\pi}\left(\frac{16}{3}-\frac{4\pi^2}{3}+4\ln\frac{m_b}{\mu}\right)\right], \tag{3.3}$$

where the lowest order contribution Γ_{77}^0 reads

$$\Gamma_{77}^0=\frac{m_b^2(\mu)m_b^3}{32\pi^4}|G_F\lambda_t C_7^{\rm eff}|^2\alpha_{\rm em}. \tag{3.4}$$

For later convenience, we can formally rewrite $\langle s\gamma|O_7|b\rangle_{\rm virt}$ in Eq. (3.1) in such a way that its square reproduces the result in Eq. (3.3). This modified matrix element, denoted by $\langle s\gamma|O_7|b\rangle_{\rm rad}$ then reads

$$\langle s\gamma|O_7|b\rangle_{\rm rad}=\langle s\gamma|O_7|b\rangle_{\rm tree}\left[1+\frac{\alpha_s}{4\pi}\left(\gamma_7\ln\frac{m_b}{\mu}+r_7\right)\right] \tag{3.5}$$

with

$$\gamma_7=\frac{8}{3},\quad r_7=\frac{8}{9}(4-\pi^2). \tag{3.6}$$

IV. VIRTUAL CORRECTIONS TO O_8

Finally, we consider the contributions to $b\to s\gamma$ generated by the operator O_8: i.e.,

$$M_8=\langle s\gamma|O_8|b\rangle. \tag{4.1}$$

The corresponding Feynman diagrams are shown in Fig. 9. The sum of the three diagrams in Fig. 9(a) yields

$$M_8[\text{Fig. 9(a)}]=\frac{Q_d C_F}{2}\frac{\alpha_s}{\pi}\left[-\frac{1}{\epsilon}-2+2\ln(m_b/\mu)-i\pi\right] \times\langle s\gamma|O_7|b\rangle_{\rm tree}, \tag{4.2}$$

while the diagrams in Fig. 9(b) give

$$M_8[\text{Fig. 9(b)}]=\frac{Q_d C_F}{12}\frac{\alpha_s}{\pi}\left[-\frac{6}{\epsilon}-21+2\pi^2+12\ln(m_b/\mu)\right] \times\langle s\gamma|O_7|b\rangle_{\rm tree}. \tag{4.3}$$

Thus, the sum of all the six diagrams is

$$M_8[\text{Fig. 9}] = \frac{Q_d C_F}{12}\frac{\alpha_s}{\pi}\Big[-\frac{12}{\epsilon} - 33 + 2\pi^2 + 24\ln(m_b/\mu) - 6i\pi\Big]\langle s\gamma|O_7|b\rangle_{\text{tree}}. \tag{4.4}$$

There is also a contribution from a counterterm; it reads

$$M_{87} = \delta Z_{87}\langle s\gamma|O_7|b\rangle_{\text{tree}}. \tag{4.5}$$

The renormalization constant

$$\delta Z_{87} = \frac{\alpha_s}{\pi} C_F Q_d \frac{1}{\epsilon} \tag{4.6}$$

has been calculated in the literature [11]. The sum of all contributions leads to the renormalized result M_8:

$$M_8 = \langle s\gamma|O_7|b\rangle_{\text{tree}}\frac{\alpha_s}{4\pi}\left(\gamma_8\ln\frac{m_b}{\mu} + r_8\right), \tag{4.7}$$

with

$$\gamma_8 = -\frac{32}{9}, \quad r_8 = -\frac{4}{27}(-33 + 2\pi^2 - 6i\pi). \tag{4.8}$$

V. RESULTS AND CONCLUSIONS

We have calculated the virtual corrections to $b\to s\gamma$ coming from the operators O_2, O_7, and O_8. The contributions from the other four-Fermi operators in Eq. (1.2), which are given by the analogous diagrams as shown in Figs. (1)–(4) were neglected, because they either vanish (O_1) or have Wilson coefficients which are about 50 times smaller than that of O_2 while their matrix elements can be enhanced at most by color factors. However, we did include the nonvanishing diagrams of O_5 and O_6 where the gluon connects the external quark lines and the photon is radiated from the charm quark because these corrections are automatically considered when C_7^{eff} [defined in Eq. (1.3)] is used instead of C_7. As discussed in Sec. III, some of the Bremsstrahlung corrections to the operator O_7 have been transferred into the matrix element for $b\to s\gamma$ in order to present results which are free from infrared and collinear singularities.

The sum of the various contributions derived in the previous sections yields the amplitude $A(b\to s\gamma)$ for $b\to s\gamma$. The result can be presented in a convenient way, following the treatment of Buras *et al.* [6], where the general structure of the next-to-leading order result is discussed in detail. We write

$$A(b\to s\gamma) = -\frac{4G_F\lambda_t}{\sqrt{2}}\hat{D}\langle s\gamma|O_7(\mu)|b\rangle_{\text{tree}}, \tag{5.1}$$

with $\hat{D}$

$$\hat{D} = C_7^{\text{eff}}(\mu) + \frac{\alpha_s(\mu)}{4\pi}\sum_i\left(C_i^{(0)\text{eff}}(\mu)\gamma_i\ln\frac{m_b}{\mu} + C_i^{(0)\text{eff}}r_i\right), \tag{5.2}$$

and where the quantities γ_i and r_i are given for $i = 2,7,8$ in Secs. II, III, and IV, respectively. For the full next-to-leading logarithmic result one would need the first term on the right-hand side (RHS) of Eq. (5.2), $C_7^{\text{eff}}(\mu)$, at next-to-leading logarithmic precision. In contrast, it is consistent to use the leading logarithmic values for the other Wilson coefficients in Eq. (5.2). As the next-to-leading coefficient C_7^{eff} is not yet known, we replace it by its leading logarithmic value $C_7^{(0)\text{eff}}$ in the numerical investigations. The notation $\langle s\gamma|O_7(\mu)|b\rangle_{\text{tree}}$ in Eq. (5.1) indicates that the explicit factor m_b in the operator O_7 is the running mass taken at the scale μ.

As the relevant scale for a b-quark decay is expected to be $\mu\sim m_b$, we expand the matrix elements of the operators around $\mu = m_b$ up to order $O(\alpha_s)$. Thus, we arrive at

$$A(b\to s\gamma) = -\frac{4G_F\lambda_t}{\sqrt{2}}D\langle s\gamma|O_7(m_b)|b\rangle_{\text{tree}}, \tag{5.3}$$

with D

$$D = C_7^{\text{eff}}(\mu) + \frac{\alpha_s(m_b)}{4\pi}\sum_i\left(C_i^{(0)\text{eff}}(\mu)\gamma_{i7}^{(0)\text{eff}}\ln\frac{m_b}{\mu} + C_i^{(0)\text{eff}}r_i\right), \tag{5.4}$$

with the quantities $\gamma_{i7}^{(0)\text{eff}}$

$$\gamma_{i7}^{(0)\text{eff}} = \gamma_i + 8\delta_{i7} \tag{5.5}$$

being just the entries of the (effective) leading order anomalous dimension matrix [6]. As also pointed out in this reference, the explicit logarithms of the form $\alpha_s(m_b)\ln(m_b/\mu)$ in Eq. (5.4) should be canceled by the μ dependence of $C_7^{(0)\text{eff}}(\mu)$. This is the crucial point why the scale dependence is reduced significantly as we will see later.[7]

From $A(b\to s\gamma)$ in Eq. (5.3), we obtain the decay width Γ^{virt} to be

$$\Gamma^{\text{virt}} = \frac{m_{b,\text{pole}}^5 G_F^2\lambda_t^2\alpha_{\text{em}}}{32\pi^4}F|D|^2, \tag{5.6}$$

where we discard term of $O(\alpha_s^2)$ in $|D|^2$. The factor F in Eq. (5.6) is

$$F = \left(\frac{m_b(\mu = m_b)}{m_{b,\text{pole}}}\right)^2 = 1 - \frac{8}{3}\frac{\alpha_s(m_b)}{\pi}. \tag{5.7}$$

To obtain the inclusive rate for $B\to X_s\gamma$ consistently at the next-to-leading order level, we have to take into account all the bremsstrahlung contributions. They have been calculated by Ali and Greub for the operators O_2 and O_7 some time ago [3], while the complete set has been worked out only recently [4,14,15]. Here, we neglect the small contribution of the operators $O_3 - O_6$ as we did for the virtual corrections;

[7] As we neglect the virtual correction of O_3–O_6, there is, of course, a small left-over μ dependence.

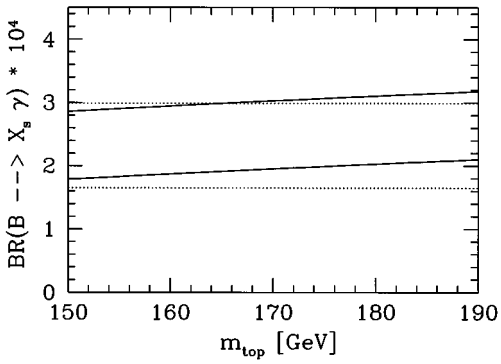

FIG. 10. Branching ratio for $b\to s\gamma$ based on the leading logarithmic formula in Eq. (5.12). The upper (lower) solid curve is for $\mu=m_b/2$ ($\mu=2m_b$). The dotted curves show the CLEO bounds [2].

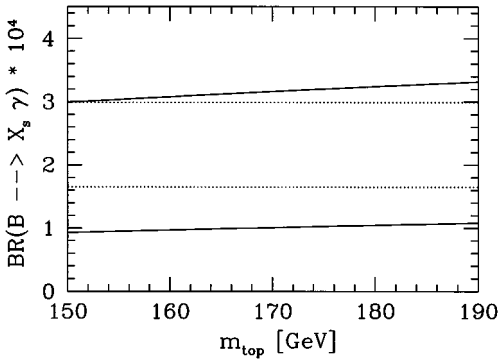

FIG. 11. Branching ratio for $b\to s\gamma(g)$ neglecting the virtual corrections of O_2 and O_8 calculated in the present paper. The upper (lower) solid curve is for $\mu=m_b/2$ ($\mu=2m_b$). The dotted curves show the CLEO bounds [2].

i.e., we only consider O_2, O_7, and O_8. The corresponding bremsstrahlung formulas are collected in Appendix B.

In order to arrive at the branching ratio $B(b\to s\gamma(g))$, we divide, as usual, the decay width $\Gamma(B\to X_s\gamma)=\Gamma^{\rm virt}+\Gamma^{\rm brems}$ by the theoretical expression for the semileptonic decay width $\Gamma_{\rm sl}$ and multiply this ratio with the measured semileptonic branching ratio $B_{\rm sl}=(10.4\pm0.4)\%$ [27], i.e.,

$$B(b\to s\gamma(g))=\frac{\Gamma}{\Gamma_{\rm sl}}\,{\rm BR}_{\rm sl}. \tag{5.8}$$

The semileptonic decay width is

$$\Gamma_{\rm sl}=\frac{G_F^2 m_{b,\rm pole}^5|V_{cb}|^2}{192\pi^3}g(m_c/m_b)\left(1-\frac{2\alpha_s(m_b)}{3\pi}f(m_c/m_b)\right), \tag{5.9}$$

where the phase space function $g(u)$ is defined as

$$g(u)=1-8u^2+8u^6-u^8-24u^4\ln u, \tag{5.10}$$

and an approximate analytic form for the radiative correction function $f(u)$ has been found in [28] to be

$$f(u)=\left(\pi^2-\frac{31}{4}\right)(1-u)^2+\frac{3}{2}. \tag{5.11}$$

In Figs. 10–12 we compare the available leading-log results and our new results for the inclusive branching ratio for $B\to X_s\gamma$ as a function of the top quark mass. A rather crucial parameter is the ratio m_c/m_b; it enters both, $b\to s\gamma$ through the virtual corrections of O_2 and the semileptonic decay width through phase space. It can be written as $m_c/m_b=1-(m_b-m_c)/m_b$. While the mass difference m_b-m_c is determined quite precisely through the $1/m_Q$ expansion [29] or from the semileptonic $b\to c$ spectrum (we use $m_b-m_c=3.40$ GeV [30]), the b-quark mass is not precisely known. Using for the b-quark pole mass $m_{b,\rm pole}=4.8\pm0.15$ GeV one arrives at $m_c/m_b=0.29\pm0.02$. In the plots the central values for $m_{b,\rm pole}$ and m_c/m_b have been used. Moreover, we put $V_{cb}=V_{ts}$ and $V_{tb}=1$ and also use the central value for the measured semileptonic branching ratio $B_{\rm sl}=10.4\%$ in Eq. (5.8). In all three plots the horizontal dotted curves show the CLEO 1σ limits for the branching ratio $B(B\to X_s\gamma)$ [2].

In Fig. 10 we show the leading logarithmic result for the branching ratio of $b\to s\gamma$, based on the formula

$$B(b\to s\gamma)^{\rm leading}=\frac{6\alpha_{\rm em}}{\pi g(m_c/m_b)}|C_7^{(0)\rm eff}|^2 B_{\rm sl}. \tag{5.12}$$

Similarly, Fig. 11 exhibits the results also taking into account the bremsstrahlung corrections and the virtual corrections to O_7 without including the virtual corrections of O_2 and O_8. We can reproduce this result by putting $\ell_2=r_2=\ell_8=r_8=0$ in our formulas. As noticed in the literature [3,15], the μ dependence in this case is even larger than that in the leading logarithmic result shown in Fig. 10. Also, the experimentally allowed region is shown.

The theoretical results shown in Figs. 10 and 11 allowed for a reasonable prediction of the branching ratio with a large error which was essentially determined by the μ dependence. As we see, they do agree well with experiment but with large uncertainties.

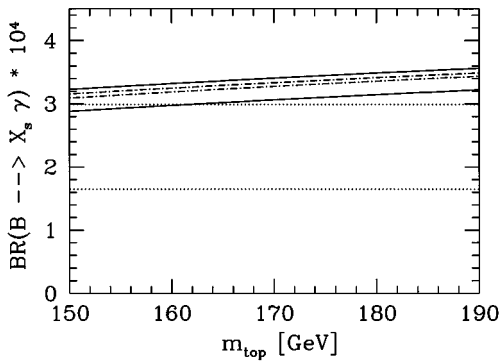

FIG. 12. Branching ratio for $b\to s\gamma(g)$ based on the complete formulas presented in this section. The band between the dash-dotted curves is obtained by taking the explicit α_s factors in Eqs. (5.4) and (5.9) at scale m_b, while the band between the solid curves corresponds to taking α_s at the (variable) scale μ. In both cases the upper (lower) curve corresponds to evaluating the Wilson coefficients at the scale $\mu=m_b/2$ ($2m_b$). For more details see text. The dotted curves show the 1σ-CLEO bounds [2].

In Fig. 12, finally, we give the branching ratio based on formula (5.8) which includes all virtual corrections calculated in the present paper. Because all the logarithms of the form $\alpha_s(m_b)\ln(m_b/\mu)$ cancel as discussed above, the μ dependence is significantly reduced in our improved calculation (Fig. 12); the bands of scale uncertainty are rather narrow. To illustrate the remaining renormalization scale dependence, we present two ''scenarios'' which differ by higher order contributions. First, we take the explicit α_s factors in Eqs. (5.4) and (5.9) at $\mu=m_b$ as indicated in these formulas; varying μ between $(m_b/2)$ and $(2m_b)$ in formula (5.4) leads to the dash-dotted curves in Fig. 12. Second, we evaluate the explicit α_s in Eqs. (5.4) and (5.9) at the (variable) scale μ. Varying again the scale μ between $(m_b/2)$ and $(2\,m_b)$ yields the solid lines in Fig. 12. In both scenarios the upper (lower) curve corresponds to $\mu=m_b/2$ ($\mu=2m_b$). We mention that the μ band is larger in the second scenario and it is, therefore, safer to use this band to obtain a feeling for the remaining scale uncertainties.

While this result shows that the theoretical accuracy can be strongly improved by the next-to-leading calculations, it would be premature to extract a prediction for the branching ratio from Fig. 12 (with obviously a small error) and claim, for instance, a discrepancy with experiment. This only will become possible (with high theoretical precision) if also $C_7^{\rm eff}$ is known to next-to-leading logarithmic precision. This additional effect will, essentially, shift the narrow bands in Fig. 12, without broadening them substantially. The drastic reduction of the theoretical uncertainties shows that significant experimental improvements are necessary to extract the important information available in these decays.

ACKNOWLEDGMENTS

We thank A. Ali, M. Beneke, R. Blankenbecler, S. Brodsky, J. Hewett, M. Lautenbacher, M. Peskin, J. Soares, and M. Worah for discussions. We are particularly indebted to M. Misiak and L. Reina for many useful comments. One of us (C.G.) would like to thank the Institute for Theoretical Physics, Zürich for the kind hospitality. This work was supported in part by Schweizerischer Nationalfonds and the U.S. Department of Energy, Contract No. DE-AC03-76SF00515.

APPENDIX A: O_2 CONTRIBUTION IN THE 't HOOFT–VELTMAN SCHEME

In this appendix we present the results for the matrix elements of the process $b\to s\gamma$ based on the operator O_2. In addition to the two-loop diagrams shown in Figs. 1–4, we also give all the counterterm contributions which multiply the Wilson coefficient C_2.

1. The 't Hooft–Veltman scheme

In the 't Hooft–Veltman scheme [13], the d dimensions are split into 4 and $d-4$; the corresponding structures are distinguished by no superscript, by a tilde, and by a hat, respectively. There are Lorentz indices in d, 4 and $d-4$ dimensions and the corresponding metric tensors $g_{\mu\nu}$, $\tilde{g}_{\mu\nu}$, and $\hat{g}_{\mu\nu}$. While all the γ matrices are taken in d dimensions, their indices are split in 4 and $d-4$ components, according to the rules

$$g_{\mu\nu}=\tilde{g}_{\mu\nu}+\hat{g}_{\mu\nu},$$

$$\tilde{g}_{\mu\nu}\tilde{g}^{\mu\nu}=4,\quad \hat{g}_{\mu\nu}\hat{g}^{\mu\nu}=d-4,$$

$$\tilde{g}_{\mu\nu}\hat{g}^{\mu\nu}=0. \tag{A1}$$

The γ matrices in four dimensions ($\tilde{\gamma}^\mu$) and $(d-4)$ dimensions ($\hat{\gamma}^\mu$) are defined by $\tilde{g}^{\mu\nu}\gamma_\nu$ and $\hat{g}^{\mu\nu}\gamma_\nu$, respectively. Assuming the usual anticommutation relations of the d-dimensional Dirac matrices in terms of the d-dimensional metric tensor $g_{\mu\nu}$, one gets the following rules for $\tilde{\gamma}^\mu$ and $\hat{\gamma}^\mu$:

$$\{\tilde{\gamma}^\mu,\tilde{\gamma}^\nu\}=2\tilde{g}^{\mu\nu},\quad \{\hat{\gamma}^\mu,\hat{\gamma}^\nu\}=2\hat{g}^{\mu\nu},\quad \{\tilde{\gamma}^\mu,\hat{\gamma}^\nu\}=0. \tag{A2}$$

The commutation relations with γ_5 are postulated to be

$$\{\tilde{\gamma}^\mu,\gamma_5\}=0,\quad [\hat{\gamma}^\mu,\gamma_5]=0, \tag{A3}$$

which is equivalent to defining γ_5 by the product $i\tilde{\gamma}_0\tilde{\gamma}_1\tilde{\gamma}_2\tilde{\gamma}_3$. This is the only way known to treat γ_5 without running into algebraic inconsistencies [31]. Finally, we mention that the chiral vertices in d dimensions can be defined in different ways, all having the same formal limit when $d\to 4$. For left- and right-handed currents we follow the common practice and use

$$\tilde{\gamma}^\mu L=R\gamma^\mu\ \ L\ \text{ and }\ \tilde{\gamma}^\mu R=L\gamma^\mu R. \tag{A4}$$

There are several possibilities to define the operators O_7 and O_8 in d dimensions (with identical four-dimensional limit); for example, the term $\sigma^{\mu\nu}$ in Eq. (1.2) can be defined to be

$$\sigma^{\mu\nu}=\frac{i}{2}[\gamma^\mu,\gamma^\nu], \tag{A5}$$

where γ^μ and γ^ν are the ''d-dimensional'' matrices, or alternatively,

$$\sigma^{\mu\nu}=\frac{i}{2}[\tilde{\gamma}^\mu,\tilde{\gamma}^\nu]. \tag{A6}$$

A difference in the definition will result in a difference of the finite terms in the one-loop matrix elements of these operators.

As the calculation of the one-loop matrix elements of O_7 and O_8 is relatively easy, once an exact definition of the operators has been specified, we give in this appendix only the result for the two-loop contribution of the operator O_2.

2. One-loop building blocks

The principal steps of the calculation in the HV scheme of the O_2 contribution to the matrix element for $b\to s\gamma$ are the same as in the NDR scheme. Therefore, we again start with the one-loop building blocks. For the building block I_β in Fig. 5, we get in the HV scheme

$$I_\beta = -\frac{g_s}{4\pi^2}\Gamma(\epsilon)\mu^{2\epsilon}\exp(\gamma_E\epsilon)\exp(i\pi\epsilon)\int_0^1 dx[x(1-x)]^{-\epsilon}$$
$$\times\left[r^2-\frac{m_c^2}{x(1-x)}+i\delta\right]^{-\epsilon}\left[x(1-x)(r_\beta r^\gamma\tilde{\gamma}_\gamma - r^2\tilde{\gamma}_\beta)\right.$$
$$\left.+\frac{m_c}{2}r^\gamma(\hat{\gamma}_\beta\tilde{\gamma}_\gamma+\tilde{\gamma}_\beta\hat{\gamma}_\gamma)\right]L\frac{\lambda}{2}, \tag{A7}$$

while the building block $J_{\alpha\beta}$ in Fig. 6 reads

$$J_{\alpha\beta}=\frac{eg_sQ_u}{32\pi^2(1+\epsilon)}R\tilde{\gamma}_\mu\left[E(\alpha,\beta,r)\Delta i_5+E(\alpha,\beta,q)\Delta i_6\right.$$
$$-E(\beta,r,q)\frac{r_\alpha}{(qr)}\Delta i_{23}-E(\alpha,r,q)\frac{r_\beta}{(qr)}\Delta i_{25}$$
$$\left.-E(\alpha,r,q)\frac{q_\beta}{(qr)}\Delta i_{26}\right]\tilde{\gamma}^\mu L\frac{\lambda}{2}-m_c\frac{eg_sQ_u}{8\pi^2}\frac{1}{(qr)}R\tilde{\gamma}_\mu$$
$$\times\{\not{r}\not{q}g_{\alpha\beta}-\gamma_\beta\not{q}r_\alpha-\gamma_\alpha\not{r}q_\beta-\gamma_\alpha\gamma_\beta\not{r}\not{q}$$
$$+\gamma_\alpha\gamma_\beta(qr)\}\tilde{\gamma}^\mu L\frac{\lambda}{2}\hat{\Delta}. \tag{A8}$$

The quantities E and Δi are given in Eqs. (2.5) and (2.6)–(2.9), respectively. As the Δi are the same as in the NDR scheme, the Ward identities in Eq. (2.12) still hold. The additional term $\hat{\Delta}$ in Eq. (A8) reads

$$\hat{\Delta}=\int_S dxdy(qr)C^{-1-\epsilon}\epsilon\Gamma(\epsilon)\mu^{2\epsilon}e^{\gamma_E\epsilon}, \tag{A9}$$

where $C^{-1-\epsilon}$ and the integration range S are defined in Eq. (2.10).

We note that the terms linear in m_c in Eqs. (A7) and (A8) are absent in schemes where γ_5 has formally the same anticommuting properties as in the four-dimensional Dirac algebra. Especially, they are absent in the NDR scheme. However, working consistently in the HV scheme, we have to retain these extra terms.

In order to make the comparison with the NDR calculation easier, we discard in a first step these extra m_c terms and denote again the corresponding results by $M_2(i)$ where $i=1,2,3,4$ numbers the figure in which the corresponding diagrams are shown. In subsections 3, 4, and 5 of Appendix A, the terms linear in m_c are left out; they are denoted by $M_2^c(i)$ and collected in subsection 6 of Appendix A. Those counterterm contributions involving evanescent operator which generate only terms linear in m_c are also discussed there.

3. Regularized two-loop contribution of O_2

We now give the results for the two-loop diagrams in Figs. 1–4 discarding the linear terms in m_c in the one-loop building blocks in Eqs. (A7) and (A8). The results read, using $z=(m_c/m_b)^2$ and $L=\ln z$,

$$M_2(1)=\left\{\frac{1}{36\epsilon}\left(\frac{m_b}{\mu}\right)^{-4\epsilon}+\frac{1}{216}[40-(540+216L)z\right.$$
$$+(216\pi^2-540+216L-216L^2)z^2$$
$$\left.-(144\pi^2+136+240L-144L^2)z^3]+\frac{i\pi}{18}[1-18z+(18-36L)z^2+(24L-20)z^3]\right\}$$
$$\times\frac{\alpha_s}{\pi}C_FQ_d\langle s\gamma|O_7|b\rangle_{\text{tree}}, \tag{A10}$$

$$M_2(2)=\left\{-\frac{1}{18\epsilon}\left(\frac{m_b}{\mu}\right)^{-4\epsilon}+\frac{1}{216}[-17+(36\pi^2-108)z\right.$$
$$-144\pi^2z^{3/2}+(648-648L+108L^2)z^2$$
$$\left.+(120\pi^2-314+12L+288L^2)z^3]\right\}$$
$$\times\frac{\alpha_s}{\pi}C_FQ_d\langle s\gamma|O_7|b\rangle_{\text{tree}}, \tag{A11}$$

$$M_2(3)=\left\{-\frac{1}{8\epsilon}\left(\frac{m_b}{\mu}\right)^{-4\epsilon}+\frac{1}{48}\{-93/2+[72-12\pi^2\right.$$
$$-96\zeta(3)+(96-24\pi^2)L+12L^2+8L^3]z$$
$$+[60+24\pi^2-96\zeta(3)+(24-24\pi^2)L$$
$$-24L^2+8L^3]z^2-(68-48L)z^3\}$$
$$+\frac{i\pi}{12}[-3+(24-2\pi^2+6L+6L^2)z$$
$$\left.+(6-2\pi^2-12L+6L^2)z^2+12z^3]\right\}$$
$$\times\frac{\alpha_s}{\pi}C_FQ_u\langle s\gamma|O_7|b\rangle_{\text{tree}}, \tag{A12}$$

$$M_2(4)=\left\{-\frac{1}{4\epsilon}\left(\frac{m_b}{\mu}\right)^{-4\epsilon}-\frac{1}{24}\{93/4+[-24+2\pi^2\right.$$
$$+24\zeta(3)-(12-6\pi^2)L+2L^3]z+[-12-4\pi^2$$
$$-48\zeta(3)+12L-6L^2+2L^3]z^2$$
$$\left.+(-6+6\pi^2-24L+18L^2)z^3\}\right\}$$
$$\times\frac{\alpha_s}{\pi}C_FQ_u\langle s\gamma|O_7|b\rangle_{\text{tree}}. \tag{A13}$$

A comparison with the corresponding NDR scheme expressions in Sec. 2 A shows that the imaginary parts are identical for each set $M_2(i)$. This property has to be satisfied because these imaginary parts can be derived by cutting rule techniques where no regularization is necessary. As expected, the only difference between the two schemes is in the m_c^2-independent terms of the real part.

4. Counterterms

There are several counterterm contributions (multiplying C_2) which all have to be taken into account. As noted, in this section we only give the counterterms whose effects do not lead to terms linear in m_c. There is just one such counterterm coming from $\delta Z_{27} O_7$. The operator renormalization constant Z_{27} [11] reads

$$\delta Z_{27} = \frac{\alpha_s}{\pi\epsilon}\left(\frac{3}{8}Q_u + \frac{1}{36}Q_d\right)C_F. \tag{A14}$$

Defining

$$M_{27} = \langle s\gamma|\,\delta Z_{27} O_7|b\rangle, \tag{A15}$$

the counterterm contribution is given by

$$M_{27} = \frac{\alpha_s}{\pi}\left(\frac{3Q_u C_F}{8} + \frac{Q_d C_F}{36}\right)\frac{1}{\epsilon}\langle s\gamma|O_7|b\rangle_{\text{tree}}. \tag{A16}$$

5. Renormalized contribution proportional to C_2

Adding the two-loop diagrams [Eqs. (A10)–(A13)] and the counterterm [Eq. (A16)], we arrive at the renormalized contribution which we denote by M_2

$$M_2 = M_2(1) + M_2(2) + M_2(3) + M_2(4) + M_{27}. \tag{A17}$$

Inserting $C_F = 4/3$, $Q_u = 2/3$, and $Q_d = -1/3$, we get in the HV scheme

$$M_2 = \langle s\gamma|O_7|b\rangle_{\text{tree}}\frac{\alpha_s}{4\pi}\left(\not{c}_2 \ln\frac{m_b}{\mu} + r_2\right), \tag{A18}$$

with

$$\not{c}_2 = \frac{416}{81}, \tag{A19}$$

$$\begin{aligned}\text{Re}r_2 = \frac{2}{243}\{&-860 + 144\pi^2 z^{3/2} + [1728 - 180\pi^2 - 1296\zeta(3)\\ &+ (1296 - 324\pi^2)L + 108L^2 + 36L^3]z + [648 + 72\pi^2\\ &+ (432 - 216\pi^2)L + 36L^3]z^2 + [-54 - 84\pi^2 + 1092L\\ &- 756L^2]z^3\},\end{aligned} \tag{A20}$$

$$\begin{aligned}\text{Im}r_2 = \frac{16\pi}{81}\{&-5 + [45 - 3\pi^2 + 9L + 9L^2]z + [-3\pi^2\\ &+ 9L^2]z^2 + [28 - 12L]z^3\}.\end{aligned} \tag{A21}$$

Again, $\text{Re}r_2$ and $\text{Im}r_2$ denote the real and the imaginary part of r_2, respectively. Comparing with the final renormalized expression M_2 in the NDR scheme, given in Sec. 2 C, we conclude again that the scheme dependence only affects the m_c^2-independent term in the real part of r_2.

6. Terms linear in m_c

Finally, we collect the linear m_c terms of the two-loop digrams which stems from in the building blocks in Eqs. (A7) and (A8). We obtain

$$\begin{aligned}M_2^c(1) = &-\frac{1}{24}\left[\frac{2}{\epsilon} + 17 - 8\ln\frac{m_b}{\mu} + 4\pi i\right]\\ &\times\frac{\alpha_s}{\pi}C_F Q_d\langle s\gamma|O_{7L}^{\text{new}}|b\rangle_{\text{tree}},\end{aligned} \tag{A22}$$

$$M_2^c(2) = -\frac{1}{24}\left[\frac{2}{\epsilon} + 11 - 8\ln\frac{m_b}{\mu}\right]\frac{\alpha_s}{\pi}C_F Q_d\langle s\gamma|O_{7R}^{\text{new}}|b\rangle_{\text{tree}}, \tag{A23}$$

$$\begin{aligned}M_2^c(3) + M_2^c(4) = &-\frac{1}{4}\left[\frac{2}{\epsilon} + 3 - 8\ln\frac{m_c}{\mu}\right]\\ &\times\frac{\alpha_s}{\pi}C_F Q_u\langle s\gamma|O_7^{\text{new}}|b\rangle_{\text{tree}},\end{aligned} \tag{A24}$$

where the newly induced magnetic type operator O_7^{new} in Eq. (A24) reads

$$O_7^{\text{new}} = m_c(\mu)\frac{e}{16\pi^2}\overline{s}\sigma_{\mu\nu}bF^{\mu\nu}. \tag{A25}$$

The operators O_{7L}^{new} or O_{7R}^{new} which only enter in intermediate steps, contain an additional left- or right-handed projection operator after the $\sigma_{\mu\nu}$ term in Eq. (A25).

In addition to these two-loop diagrams, there are two counterterms proportional to evanescent operators which lead to terms linear in m_c. The first (denoted by $1/\epsilon O_{4\,\text{Fermi}}^{\text{ev}}$) comes from one-loop gluon corrections to the four-Fermi operator O_2 and is given explicitly in Ref. [32]. As we use this operator only as an insertion into the matrix element for $b\to s\gamma$, we adapt the general color structure given in [32] for this special case. In our notation, this counterterm takes the form

$$\frac{1}{\epsilon}O_{4\,\text{Fermi}}^{\text{ev}} = -\frac{\alpha_s}{8\pi\epsilon}\frac{1}{C_F}\,\text{E}_{\text{HV}}, \tag{A26}$$

with

$$\begin{aligned}\text{E}_{\text{HV}} = &-12\epsilon(\Gamma_-\otimes\Gamma_+ + \Gamma_+\otimes\Gamma_-) - [\tilde{\gamma}_\tau\tilde{\gamma}_\rho\hat{\gamma}_\mu\gamma_5\\ &\otimes\tilde{\gamma}^\tau\tilde{\gamma}^\rho\hat{\gamma}^\mu\gamma_5 + 2\hat{\gamma}_\mu\otimes\hat{\gamma}^\mu - 2\hat{\gamma}_\mu\gamma_5\otimes\hat{\gamma}^\mu\gamma_5]\\ &-[\gamma_\mu\gamma_\rho\Gamma_-\gamma^\rho\gamma^\mu\otimes\Gamma_- - \gamma_\mu\gamma_\rho\Gamma_-\otimes\Gamma_-\gamma^\rho\gamma^\mu\\ &-\Gamma_-\gamma_\rho\gamma_\mu\otimes\gamma^\mu\gamma^\rho\Gamma_- + \Gamma_-\otimes\gamma_\mu\gamma_\rho\Gamma_-\gamma^\rho\gamma^\mu],\end{aligned} \tag{A27}$$

where $\Gamma_\pm = \tilde{\gamma}_\mu(1\pm\gamma_5)/2$. Its contribution to the amplitude for $b\to s\gamma$ is

$$M_2^{\text{ev}}[\text{ four Fermi}] = \left(\frac{1}{\epsilon} - 2\ln\frac{m_c}{\mu}\right)\frac{\alpha_s}{\pi}C_F Q_u\langle s\gamma|O_7^{\text{new}}|b\rangle_{\text{tree}}. \tag{A28}$$

The second counterterm (denoted by $1/\epsilon O^{\rm ev}_{\rm penguin}$) corresponds to the $1/\epsilon$ pole term in m_c term in the one-loop building block I_β in Eq. (A7). It can be written as

$$\frac{1}{\epsilon}O^{\rm ev}_{\rm penguin}=\frac{1}{\epsilon}\frac{g_s}{16\pi^2}m_c\overline{sR}\sigma_{\mu\nu}L\frac{\lambda^A}{2}bG_A^{\mu\nu}. \quad \text{(A29)}$$

Its contribution to the amplitude $b\to s\gamma$ is given by six graphs whose Feynman diagrams are similar to those shown in Fig. 9. The three diagrams, where the gluon is absorbed by the s quark, read

$$M_2^{\rm ev}(\text{penguin } a)=\frac{1}{36}\left[\frac{6}{\epsilon}+19-12\ln\frac{m_b}{\mu}+6\pi i\right]\times\frac{\alpha_s}{\pi}C_FQ_d\langle s\gamma|O_{7L}^{\rm new}|b\rangle_{\rm tree}, \quad \text{(A30)}$$

while the diagrams where the gluon is absorbed by the b quark is given by

$$M_2^{\rm ev}(\text{penguin } b)=\frac{1}{18}\left[\frac{3}{\epsilon}+5-6\ln\frac{m_b}{\mu}\right]\times\frac{\alpha_s}{\pi}C_FQ_d\langle s\gamma|O_{7R}^{\rm new}|b\rangle_{\rm tree}. \quad \text{(A31)}$$

Adding the contributions of the two-loop diagrams in Eqs. (A22)–(A24) and the counterterm contributions in Eqs. (A28), (A30), and (A31), we end up with a total linear m_c term of the form

$$M_2^c[\text{two loop + counterterm}]=\frac{\alpha_s}{\pi}C_F\left[\frac{Q_d}{72}\left(\frac{6}{\epsilon}-13\right)+\frac{Q_u}{4}\left(\frac{2}{\epsilon}-3\right)\right]\langle s\gamma|O_7^{\rm new}|b\rangle_{\rm tree}. \quad \text{(A32)}$$

Of course, this result can be made finite by introducing a corresponding counterterm proportional to $O_7^{\rm new}$ given in Eq. (A25) which minimally subtracts the $1/\epsilon$ pole in Eq. (A32).

At this point one might ask why these additional operators appearing in this subsection do not appear in the literature [11] where the singularity structure of these graphs have been worked out in order to extract the $O(\alpha_s)$ anomalous dimension matrix. We also note that there are other new operators induced if one looks, e.g., at the analogous two-loop corrections to $b\to s\gamma$ associated to other four-Fermi operators. For example, the corrections to O_3 generate a new magnetic-type operator, where m_c in Eq. (A25) is replaced by m_b.

To absorb all the divergencies, one clearly has to enlarge the operator basis in this scheme. However, we believe that it is correct to ignore these additional operators for the leading logarithmic result for $b\to s\gamma$. The reason is the following: First, the new operators do not mix into the old ones given in Eq. (1.2) at $O(\alpha_s)$; therefore, the old operators run in the same way with or without including the new operators. Second, in the $O(\alpha_s^0)$ matching (at $\mu=m_W$), the new coefficients have to be zero, as one can easily see. Third, the absence of a $\ln(\mu)$ term in Eq. (A32) indicates that the four-Fermi operators do not induce any running of the new operators at the leading logarithmic level. The only way the new magnetic operators could run is by multiplicative renormalization. But as these operators have zero initial value as discussed above, this effect also is unimportant: To leading logarithmic precision the Wilson coefficients of the new operators are zero at each renormalization scale. Therefore, the new operators certainly do not change the leading logarithmic physics. Equivalently, one can say that one can throw away the terms proportional to m_c in the building blocks in Eqs. (A7) and (A8) when working at leading order.

However, our result in Eq. (A32) shows that the matrix element of O_2 leads to finite terms (which are of next-to-leading order) linear in m_c when calculated in the HV scheme. It would be very interesting to see if these linear m_c terms are canceled by the next-to-leading Wilson coefficients of the new operators. Such a cancellation is expected to occur, of course, because in any other scheme which respects the four-dimensional chirality properties, these terms do not appear.

APPENDIX B: BREMSSTRAHLUNG CORRECTIONS

In order to make the paper self-contained, we give in this appendix the formulas for the process $b\to s\gamma g$ based on the operators O_2, O_7, and O_8 in the NDR scheme. As we have given the analogous virtual corrections to $b\to s\gamma$ in the limit $m_s\to 0$, we also present the bremsstrahlung corrections for this case.

We denote the various contributions to the bremsstrahlung decay width Γ^b by Γ^b_{22}, Γ^b_{77}, Γ^b_{88}, Γ^b_{27}, Γ^b_{28}, Γ^b_{78}; for example, Γ^b_{22} is based on the matrix element squared of O_2, while Γ^b_{27} is an interference term between the matrix element of O_2 and O_7, etc.

Note that all the interference terms and Γ^b_{22} are infrared (and collinear) finite. The sum of these four finite contributions is given by

$$\Gamma_F^{\rm brems}=\frac{G_F^2|\lambda_t|^2\alpha_{em}\alpha_s}{768\pi^5 m_b}\int_{PS}dE_g dE_\gamma(\tau_{22}+\tau_{27}+\tau_{28}+\tau_{78}), \quad \text{(B1)}$$

$$\tau_{22}=2m_b^2Q_u^2C_2^2(\mu)|\kappa|^2[m_b^2-2(qr)], \quad \text{(B2)}$$

$$\tau_{27}=-32m_b^2Q_uC_2(\mu)C_7^{\rm eff}(\mu)(qr)\mathrm{Re}(\kappa), \quad \text{(B3)}$$

$$\tau_{28}=-32m_b^2Q_uQ_dC_2(\mu)C_8^{\rm eff}(qr)\mathrm{Re}(\kappa), \quad \text{(B4)}$$

$$\tau_{78}=-128m_b^2Q_dC_7^{\rm eff}(\mu)C_8^{\rm eff}(\mu)(qr)\frac{m_b^4+2(pq)(pr)}{(pq)(pr)}, \quad \text{(B5)}$$

where as in the previous sections p, p', q, and r denote the four-momenta of the b and the s quark, the photon, and the gluon, respectively. The function κ is defined as

$$\kappa=\frac{4[2G(t)+t]}{t},\quad t=\frac{2(qr)}{m_c^2}, \quad \text{(B6)}$$

$$G(t)=\int_0^1 \frac{dy}{y}\ln[1-ty(1-y)-i\epsilon]. \tag{B7}$$

The phase space boundaries (denoted above by PS) are given by

$$E_\gamma \in \left[0,\frac{m_b}{2}\right], \quad E_g \in \left[\frac{m_b}{2}-E_\gamma,\frac{m_b}{2}\right]. \tag{B8}$$

Note that the function κ in Eq. (B6) is finite for $m_c \to 0$. Therefore, also the bremsstrahlung corrections have a finite limit for $m_c \to 0$.

Γ_{77}^b is singular for $E_g \to 0$ or $\vec{r} \| \vec{p}\,'$. As it cancels the corresponding singularity of the virtual corrections to O_7, we have taken into account the contribution Γ_{77}^b already in Sec. III, i.e., Γ_{77}^b is contained in the finite quantity in Eq. (3.3).

Finally, Γ_{88}^b is singular for $E_\gamma \to 0$ or $\vec{q} \| \vec{p}\,'$. These singularities can be removed by adding the virtual photon corrections to $b \to sg$. This finite sum Γ_{88} can easily be obtained from Γ_{77} in Eq. (3.3). It reads

$$\Gamma_{88}=\frac{m_b^5}{96\pi^5}|G_F Q_d C_8^{\rm eff}\lambda_t|^2 \alpha_{\rm em}\alpha_s\left(\frac{16}{3}-\frac{4\pi^2}{3}+4\ln\frac{m_b}{\mu}\right). \tag{B9}$$

To summarize, the total inclusive decay width Γ for $B \to X_s+\gamma$ is then given by $\Gamma=\Gamma^{\rm virt}+\Gamma_F^{\rm brems}+\Gamma_{88}$, where $\Gamma^{\rm virt}$, $\Gamma_F^{\rm brems}$, and Γ_{88} are given in Eqs. (5.6), (B1), and (B9), respectively.

[1] CLEO Collaboration, R. Ammar *et al.*, Phys. Rev. Lett. **71**, 674 (1993).
[2] CLEO Collaboration, M.S. Alam *et al.*, Phys. Rev. Lett. **74**, 2885 (1995).
[3] A. Ali and C. Greub, Z. Phys. C **49**, 431 (1991); Phys. Lett. B **259**, 182 (1991); **287**, 191 (1992); Z. Phys. C **60**, 433 (1993).
[4] A. Ali and C. Greub, Phys. Lett. B **361**, 146 (1995).
[5] R.D. Dikeman, M. Shifman, and R.G. Uraltsev, Int. J. Mod. Phys. A **11**, 571 (1996).
[6] A.J. Buras, M. Misiak, M. Münz, and S. Pokorski, Nucl. Phys. **B424**, 374 (1994).
[7] M. Ciuchini *et al.*, Phys. Lett. B **334**, 137 (1994).
[8] J.M. Soares, Phys. Rev. D **49**, 283 (1994).
[9] B. Grinstein, R. Springer, and M.B. Wise, Phys. Lett. B **202**, 138 (1988); Nucl. Phys. B **339**, 269 (1990).
[10] T. Inami and C.S. Lim, Prog. Theor. Phys. **65**, 297 (1981).
[11] M. Ciuchini *et al.*, Phys. Lett. B **316**, 127 (1993); Nucl. Phys. **B415**, 403 (1994); G. Cella *et al.*, Phys. Lett. B **325**, 227 (1994); M. Misiak, Nucl. Phys. **B393**, 23 (1993); **B439**, 461(E) (1995).
[12] A. Ali, G. Giudice, and T. Mannel, Z. Phys. C **67**, 417 (1995).
[13] G. 't Hooft and M. Veltman, Nucl. Phys. **B44**, 189 (1972).
[14] A. Ali and C. Greub (in preparation).
[15] N. Pott, Phys. Rev. D **54**, 938 (1996).
[16] K. Adel and Y.-P. Yao, Phys. Rev. D **49**, 4945 (1994).
[17] *Pocketbook of Mathematical Functions*, edited by M. Abramowitz and Irene Stegun (Verlag Harri Deutsch, Frankfurt/Main, 1984).
[18] H. Simma and D. Wyler, Nucl. Phys. **B344**, 283 (1990).
[19] E.E. Boos and A.I. Davydychev, Theor. Math. Phys. **89**, 1052 (1992).
[20] N.I. Usyukina, Theor. Math. Phys. **79**, 385 (1989); **22**, 211 (1975).
[21] V.A. Smirnov, *Renormalization and Asymptotic Expansions* (Birkhäuser, Basel, 1991).
[22] *Higher Transcendental Functions*, edited by A. Erdelyi (McGraw-Hill, New York, 1953).
[23] J.M. Soares, Nucl. Phys. **B367**, 575 (1991).
[24] A.C. Hearn, REDUCE *User's Manual* (Rand, Santa Monica, California, 1987).
[25] M. Jamin and M.E. Lautenbacher, Comput. Phys. Commun. **74**, 265 (1993); **74**, 11 (1993); **74**, 39 (1993); **74**, 55 (1993).
[26] A. Heck, *Introduction to* MAPLE (Springer-Verlag, New York, 1993).
[27] CLEO Collaboration, L. Gibbons, in Proceedings of the XXX Rencontres de Moriond, Les Arcs (unpublished).
[28] G. Corbo, Nucl. Phys. **B212**, 99 (1983); N. Cabibbo, G. Corbo, and L. Maiani, *ibid.* **B155**, 93 (1979).
[29] I. Bigi *et al.*, Phys. Rev. Lett. **71**, 496 (1993).
[30] M. Shifman, N.G. Uraltsev, and A. Vainshtein, Phys. Rev. D **51**, 2217 (1995); M.B. Voloshin, Report No. TPI-MINN-94/38-T, hep-ph/9411296 (unpublished).
[31] P. Breitenlohner and D. Maison, Commun. Math. Phys. **52**, 11 (1977); **52**, 39 (1977); **52**, 55 (1977).
[32] A.J. Buras and P.H. Weisz, Nucl. Phys. **B333**, 66 (1990).